Type of the Paper: Article

PTA-based ruthenium complexes as photosensitizers for dye-sensitized solar cells

Benjamin Sierra-Martin[1,*], Ana Maldonado-Valdivia[1], Manuel Serrano-Ruiz[2], Antonio Romerosa[2] and Antonio Fernandez-Barbero[1]

1 NanoLab, Department of Chemistry and Physics, University of Almeria, 04120 Almeria, Spain; bsierra@ual.es, amaldonado@ual.es, afernand@ual.es
2 Inorganic Chemistry Lab, Department of Chemistry and Physics, University of Almeria, 04120 Almeria, Spain; mserrano@ual.es, romerosa@ual.es
* Correspondence: bsierra@ual.es; Tel.: +34-950015909

Received: date; Accepted: date; Published: date

Abstract: Two novel ruthenium complexes are synthesized and used as photosensitizers in dye-sensitized solar cells (DSCs): $[RuCl_2(mPTA)_3(H_2O)](CF_3SO_3)_3$ (C1) (m: methyl; PTA: 3,5,7-triaza-phosphaadamantane) and $[Ru(C{=}C{=}CPh_2)Cp(PTA)(PPh_3)](CF_3SO_3)$ (C2). The complexes are soluble in organic solvents and, interestingly, in water, which makes them useful for water-based photochemical processes. They possess excellent photon-absorption properties over a wide range of the UV-vis spectrum with intense peaks at ~ 330 nm for both sensitizers and a second peak for C2 at 525 nm, much stronger than the corresponding to dye N719. The performance of DSCs containing these sensitizers are evaluated using different electrolytes in comparison with a reference cell made with N719. The solar cell performance was similar for both complexes and strongly dependent on the electrolyte, with a maximum conversion efficiency of 0.33 % for the iodide/triiodide electrolyte. In spite of presenting low efficiencies, these novel ruthenium dyes produce electricity from light effectively and are highly stable under irradiation conditions.

Keywords: ruthenium complex, dye, sensitizer, solar cell, PTA.

1. Introduction

The use of dye-sensitized solar cells (DSCs) is a well stablished strategy for solar energy conversion because of their high efficiency, inexpensive manufacturing and environmental friendly nature [1,2]. DSCs are sandwich-type electrochemical devices based on nanocrystalline metal oxide semiconductors sensitized by molecular dyes [3,4]. The dye (or photosensitizer) is able to absorb a wide range of the solar spectrum to reach its excited state, then producing photoelectrons that are injected directly into the conduction band of the semiconductor (photoelectrode). The semiconductor often consists of a mesoporous TiO_2 film deposited on a transparent fluorine-doped tin oxide (FTO) conducting glass; this provides a large surface area to maximize the light adsorption while ensures the electrical connection dye-electrolyte. The injected electron flow towards the counter electrode, a platinized FTO glass substrate, where they are transferred to the redox pair present in the electrolyte (usually I^-/I_3^-). The circuit is completed when the oxidized dye is regenerated to its ground state by electron donation from the electrolyte. As a result, DCSs perform an electrical work through a regenerative photo-electrochemical cycle without consumption of chemical species [5].

DSCs use indistinctly natural or synthetic dyes to harvest energy from light [6]. Artificial dyes, usually based on transition metal coordination complexes such as Ru, Os, Pt are the most widely employed since they yield greater efficiencies [7,8]. Ruthenium-based complexes satisfy a few key requirements to work properly, such as photon absorption across a broad range of wavelengths, chelation to TiO_2 surface, and chemical stability. Among these complexes, polypyridyl ruthenium dyes such as the well-known N719, N3, N749 have been widely used and studied for their broad-spectrum absorption, excellent redox characteristics and high stability. Moreover, they strongly

bound to the mesoporous TiO_2 film through carboxylate or phosphonate groups, ensuring efficient electron injection into the photoelectrode. So far, these dyes have achieved conversion efficiencies >11 % and are considered as benchmark reference sensitizers [9–11].

At present, considerable development is focused on the design of novel dye structures to enhance the dye-sensitized solar cell performance [12]. Progress in the optimization of the dye is usually performed through systematic variation of the ligands and other substituent groups [13,14]. This strategy allows to control the photon absorption properties as well as the electronic coupling between the sensitizer excited state and the semiconductor conduction band, which in turn determine the efficiency of the solar cell. Advances on the design of ruthenium-based dyes and their applications in DSCs have been extensively reviewed [15–18].

In this work, two PTA-based ruthenium complexes are synthesized and investigated as photosensitizers in DSCs: $[RuCl_2(mPTA)_3(H_2O)](CF_3SO)_3$ and $[Ru(C{=}C{=}CPh_2)Cp(PTA)(PPh_3)](CF_3SO_3)$, with m: methyl and PTA: 3,5,7-triaza-phosphaadamantane. The presence of PTA ligands made these complexes soluble in aqueous solvents, which makes them useful for water-based photochemical processes. In regard to the Uv-vis properties, both complexes present an intense absorption band at ~ 330 nm while complex 2 displays a much stronger absorption at 525 nm. Moreover, the chelation of these dyes to the titania film can be accomplished via the PTA groups, similarly to the anchoring provided by phosphate groups [19]. The efficiency of DSCs containing the complexes in combination with three electrolytes is evaluated in comparison with the standard dye N719. The electrochemical behavior was similar for both complexes with a strong influence of the electrolyte. Overall, we found a maximum conversion efficiency for the DSCs of ~ 0.33 %. However, despite the low efficiencies, these new dyes produce electricity from light effectively and are chemically stable under irradiation.

2. Materials and Methods

2.1. Materials

Conducting glass plates (FTO) (F-doped SnO_2, with resistance 11–13 Ω/sq, Nippon Sheet Glass) were used to fabricate the electrodes of the DSCs. Nanocrystalline TiO_2 (P-25, Degussa), Triton X-100 (Merck) and H_2PtCl_6 (Aldrich) were used for preparing the TiO_2 and Pt films onto the FTO plates. Iodine (99.9%, Aldrich), LiI (99.9%, Aldrich), 4-tert-butylpyridine (TPB) (96%, Aldrich), 1-methyl-3-propylimidazolium iodide (MPII) (98%, Aldrich), N-Methylbenzimidazole (NMBI) (99%, Aldrich), Guanidinium thiocyanate (GNCS) (99%, Sigma) and 3-methoxypropionitrile (98%, Aldrich) were employed to prepare the electrolyte solutions. The dye N719 (95%) and all the other chemicals were purchased from Sigma-Aldrich with reagent grade and used as received.

2.2. Synthesis of the ruthenium complexes

All reactions were carried out under a dry nitrogen atmosphere by using standard Schlenk-tube techniques. The solid complexes were collected on sintered glass-frits and subsequently washed as described. The following products required for the synthesis were prepared according to literature procedures: PTA [20], $[RuCl_2(PPh_3)_2]$ [21,22], [RuCpCl(PPh3)2][23] and [RuCpCl(PTA)(PPh3)] [24,25].

2.2.1. Synthesis of complex 1: $[RuCl_2(mPTA)_3(H_2O)](CF_3SO_3)_3$

We first performed the preparation of the compound $mPTA(CF_3SO_3)$, which is one of the reactants to accomplish the synthesis of complex 1. To this end, $MeCF_3SO_3$ (0.56 mL, 5.08 mmol) was added to a stirred PTA (0.6 g, 3.82 mmol) solution prepared in $CHCl_3$ (60 mL). A white suspension is formed, which was further stirred for 30 min at room temperature. The resulting white precipitate was filtered, washed with $CHCl_3$ and air-dried. Yield: 91.3%.

Complex 1 was synthesized by reaction among $mPTA(CF_3SO_3)$ and $[RuCl_2(PPh_3)_2]$ in MeOH according to Scheme I. The complex $[RuCl_2(PPh_3)_2]$ (450 mg, 0.47 mmol) was dissolved in MeOH (60 mL) and then $mPTA(CF_3SO_3)$ (460 mg, 1.43 mmol) was added. The MeOH used for the synthesis was not previously dried, providing the water source necessary for the reaction. After 6 h of reaction at room temperature, a yellow–orange solution was obtained. Next, the solvent was reduced to 15 mL

and 20 mL of Et_2O were added. The yellow precipitate formed was filtered under inert atmosphere, washed with Et_2O and dried under vacuum. Yield: 84%.

The yellow complex 1 is soluble and stable in water ($S_{25\,°C}$ = 89 mg mL^{-1}) at room temperature and also in the dark. The molecular structure consists of a distorted octahedral ruthenium atom bonded to two mPTA trans to each other, two Cl ligands trans to each other and one mPTA trans to one water molecule [26]. The positive charge of the complex is balanced by three $CF_3SO_3^-$ counter-ions. To the best of our knowledge, this complex is the first reported example in which one mPTA is trans to a H_2O molecule [27].

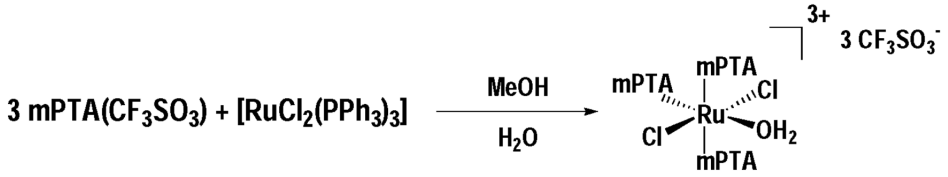

Scheme I. Synthesis of the ruthenium complex 1 (C1).

2.2.2. Synthesis of complex 2: $[Ru(C{=}C{=}CPh_2)Cp(PTA)(PPh_3)](CF_3SO_3)$

The allenylidene-ruthenium complex was prepared following the Scheme II. In the synthetic process, $Ag(CF_3SO_3)$ (0.03 g, 0.12 mmol) dissolved in $CHCl_3$ (2 mL) was added to a stirred solution of $[RuCpCl(PTA)(PPh_3)]$ (0.072 g, 0.12 mmol) prepared in 30 mL of $CHCl_3$. The solution was reacted with 1,1-diphenyl-2-propyn-1-ol (0.18 g, 0.81mmol) for 5 min at room temperature followed by 2 h of reaction at refluxing temperature. The resulting mixture was filtered to remove the precipitated AgCl, yielding a purple solid after the solvent evaporation. The solid, which corresponds to the ruthenium complex 2 was washed with Et_2O (2 x 5 mL) and dried under vacuum before use. Yield: 0.10 g (94%).

Complex 2 is soluble in common organic solvents and slightly soluble in water ($S_{25\,°C}$ = 0.1 mg mL^{-1}). The formation of the complex is confirmed by $^{13}C\{^1H\}$ NMR. The spectrum reveals a neat triplet slightly below 293.7 ppm that corresponds to the allenylidene α-carbon coupled to the two phosphines P-atoms. Moreover, signals ascribable to both β- and γ-carbons are detected at the expected chemical shifts. The complex keeps its nature in the solid state, as confirmed by the characteristic allenylidene stretching absorption band observed in the solid IR spectra, $\nu_{(C=C=C)}$: 1930 cm^{-1}. The structure is tackled trough the X-ray analysis of crystals made of their parent complex, $[RuCp(DMSO\kappa S)(PTA)(PPh_3)]$. The calculated cone angle are 133° for the PPh_3 and 109° for the PTA, in agreement with those found for other ruthenium complexes with PPh_3 and PTA ligands [28].

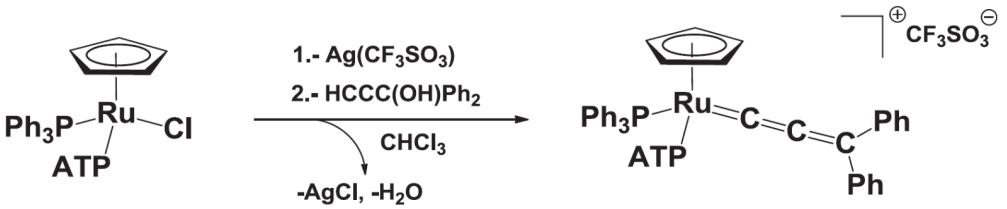

Scheme II. Synthesis of the ruthenium complex 2 (C2).

2.3. FTO electrical resistance

The influence of the thermal treatment on the electrical resistance, R, of FTO glass substrates was studied following the Van der Pauw method [29]. Before any treatment R_S = (12.60 ± 0.20) Ω/sq, whereas after the cleaning process (isopropanol) and activation with temperature (420 °C, 30 min) the value was Rs = (13.45 ± 0.15) Ω/sq. The FTO is then a suitable material for solar cell fabrication, provided that the thermal treatment does not increase significantly the sheet resistance; this, in turn, ensures the solar cell performance [30].

2.4. Fabrication of the photoelectrodes

A concentrated paste of TiO_2 (15 wt.%) was prepared by dispersing TiO_2 nanoparticles (diameter = 20 nm) in a mixture of ethanol (61 wt.%) and nitric acid (24 wt.%) under 12 h of continuous stirring at room temperature. The surfactant Triton X-100 (0.2 wt.%) was added and the mixture stirred for additional 12 h.

To fabricate the photoelectrode, FTO substrates were covered with transparent adhesive tape (Scotch, 50 μm in thickness), leaving a square-shaped free surface of ~ 0.5 cm^2. A drop of the TiO_2 paste was spread using a glass rod over the square area by the so called doctor-blade technique. The paste was allowed to dry at room temperature for 1h under ethanol atmosphere. Next, the substrate was placed in a muffle furnace (450 °C, 1 h) to calcine the paste, then creating the mesoporous TiO_2 film. This procedure yields high quality TiO_2 films without granular features or cracks on the surface [31].

The different ruthenium complexes were absorbed onto the TiO_2 film by adding an excess of the dye solution with the titania film facing up. The dye N719 was prepared in ethanol at 3.10^{-4} M, C1 in H_2O at 3.10^{-2} M, and C2 in chloroform at 3.10^{-3} M. The absorption process was conducted in dark at room temperature for 24 h. The non-adsorbed dye was removed by rinsing the stained titania with ethanol.

The platinized counter electrode was made by coating the FTO substrate with a thin layer of Pt. A droplet of the H_2PtCl_6 solution (0.01 M in ethanol) was spread on the surface, followed by a thermal process in air at 380 °C during 20 min.

2.5. DSC assembly and chraracterization

The solar cells were assembled following the procedure stablished by Ito et al. [32,33]. The dye-sensitized electrode and the counter electrode were put together in a sandwich-type cell using a thermal adhesive film (Dupont Surlyn, 60 μm) to set the gap between the two electrodes and make the solar cell airtight. The electrolytes were introduced in the gap by capillarity from a tiny hole drilled on the counter electrode. As a result of the manufacturing process, we obtain DSCs with an active electrode area of about 0.36 cm^2.

Figure 1 shows DSCs prepared with the ruthenium complexes; the pale yellow cell (left) corresponds to complex 1 whereas complex 2 produces a red cell (right) analogous in color to the solar cell prepared with N719. Note the high transparency of the FTO plates and the fact that the two glass substrates are slightly shifted in order to leave room for the electrical contacts.

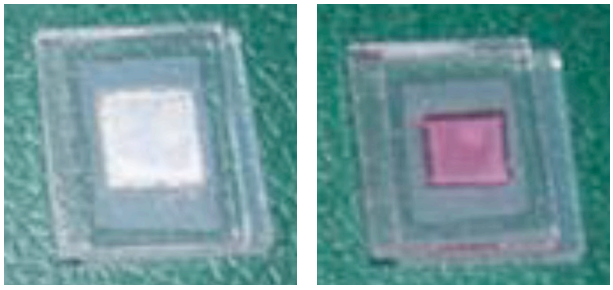

Figure 1. Dye-sensitized solar cells prepared with the ruthenium complexes C1 (left) and C2 (right).

Photocurrent–voltage (I–V) curves for the DSCs were measured under direct sun radiation in shiny days at noon time. Under these conditions, the solar irradiation was about 800 W/m^2 in all tests. The light irradiation was determined by a thermopile-based pyranometer. The I–V curves were determined by digital source meters without any external bias. The electrical data were averaged over three samples in each case, which also allowed to check the result reproducibility.

3. Results and Discussion

3.1. UV-visible properties

The UV-vis absorption spectra were recorded using a high resolution diode array spectrophotometer (HR4000, Ocean Optics). Figure 2 plots the normalized absorption vs wavelength of the ruthenium complexes, including the well-known spectrum of N719 in ethanol. The electronic spectrum of complex 1 in water is characterized by a strong absorption peak at 326 nm and a smaller peak at 448 nm; the absorption coefficient was $\varepsilon_{max} \approx 10^3$ $M^{-1}cm^{-1}$. On the other hand, complex 2 in chloroform displays a peak at 338 nm and a broad and intense absorption band in the visible range, with the maximum located at 520 nm. This band perfectly matches with one absorption peaks of the dye N719, but it is much stronger for the complex 2. Furthermore, the first peak of both dyes appears at similar wavelengths than the corresponding to the maximum absorption of N719 (315 nm).

The electronic properties of the ruthenium complexes arise from ligand-centered charge transfer transitions (LCCT), as well as metal-to-ligand charge transfer transitions (MLCT). The absorption peaks at higher wavelengths (visible range) arise from the MLCT transitions, while the more energetically demanding LCCT transitions give rise to the absorption in the UV region [34]. In general, the novel ruthenium complexes show absorption properties similar to that of complex N719, with strong absorption bands covering a wider range of the spectrum. To be effective, a dye must be excited over a wide range of wavelengths in addition to present a high absorption coefficient. In view of these results, the ruthenium complexes seem to meet the requirements to be sensitizers for DSCs.

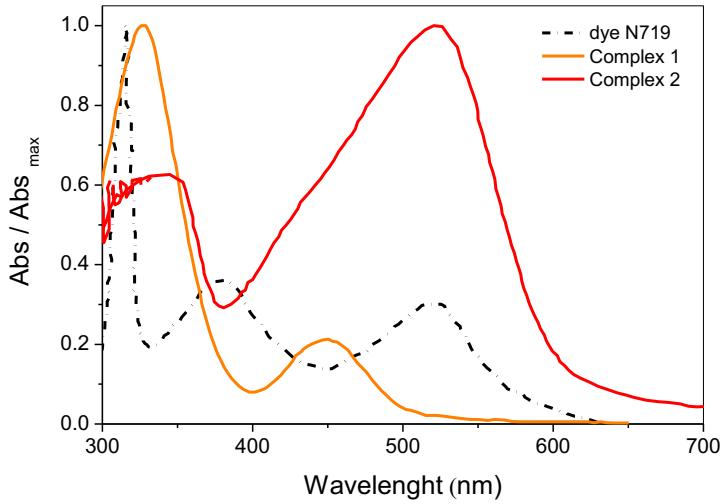

Figure 2. UV-visible absorption spectra of the ruthenium complexes; N719 was prepared in ethanol at 3.10^{-4} M, complex 1 in H_2O at 3.10^{-2} M, and complex 2 in chloroform at 3.10^{-3} M.

3.2. Morphology of the Pt electrode

Atomic Force Microscopy (AFM) was used to characterize the morphology, topography and roughness of the counter electrode as these parameters strongly affect to the solar cell performance. Figure 3 shows an AFM image of the surface of the Pt film deposited on the FTO substrate. The image was taken with a microscope Veeco Innova (model 840-012-711) in tapping mode by scanning an area of 3 μm × 3 μm with 1024 lines resolution at a scan rate of 0.6 μm/s. The image shows a highly textured Pt electrode with a surface roughness of 32.3 nm. For the scanned surface (9.0 μm^2) the resulting surface area was 12.60 μm^2 (surface/area ratio = 1.4). Our results are very similar to the obtained by Tsai and coworkers [35]. These authors found the best solar cell performance for platinized electrodes with roughness = 28.3 nm and surface/area ratio = 1.17. This confirms that our deposition method optimizes the morphology of the Pt counter electrode. The resulting high roughness and surface area enhances the catalytic ability of the electrode for I_3^- ions reduction and the charge exchange at the

209 Pt/electrolyte interface. As a result, the conversion efficiency of solar cell is expected to enhance by
210 10% respect to other electrode morphologies [35].
211

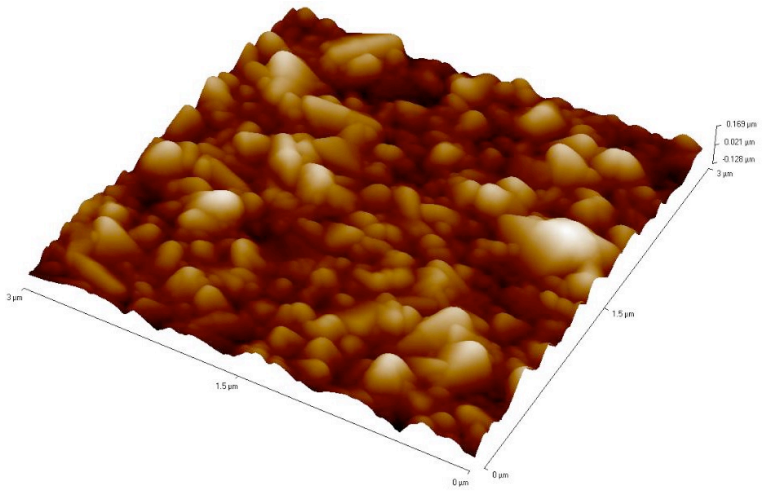

212
213 **Figure 3**. AFM image of the platinized counter electrode. Scan was performed in tapping mode at
214 0.6 µm/s covering an area of 3 µm × 3 µm.

215 *3.3. Solar cell performance*

216 The manufactured cells are named as Cx-ELy, being x, y the numbers of the complex (C) and
217 electrolyte (EL), respectively. Three electrolytes with the following compositions were used: EL1:
218 0.05 M I_2, 0.5 M LiI, 0.5 M 4-tert-butylpyridine (TBP) in 3-methoxypropionitrile; EL2: 0.05 M I_2, 0.5 M
219 LiI in 3-methoxypropionitril; EL3: 1.0 M PMII, 0.5 M NMBI, 0.1 M GNCS in 3-methoxypropionitrile.
220 Electrolytes 1, 2 are based on the iodide/triiodide redox couple because it is considered one of the
221 most efficient charge mediator [30]. Electrolyte 3 is a liquid ionic composed of imidazolium salts as a
222 source of iodide and it is widely used because of their improved chemical and thermal stability, which
223 is a key requirement for long-lived DSCs [36]. For each combination of complex-electrolyte, at least
224 three solar cells were fabricated in order to confirm the reproducibility of the results.
225 Figure 4 shows average photocurrent–V curves of the DSCs fabricated with each one of the
226 ruthenium complexes. The curves allow to access the electrical parameters: open circuit voltage, V_{OC};
227 short circuit current, I_{SC}; fill factor, FF; and overall efficiency, η, which represents the percentage
228 amount of solar light converted in electrical output. These parameters are obtained averaging
229 measures from at least three DSCs and summarized in Table 1. For comparison, a reference cell is
230 made with the dye N719 and electrolyte 1 (N719-E1). The reference cell yields an efficiency close to
231 11%, as expected according to previous works [33,37]; this result validates our manufacturing process
232 of the solar cells.
233

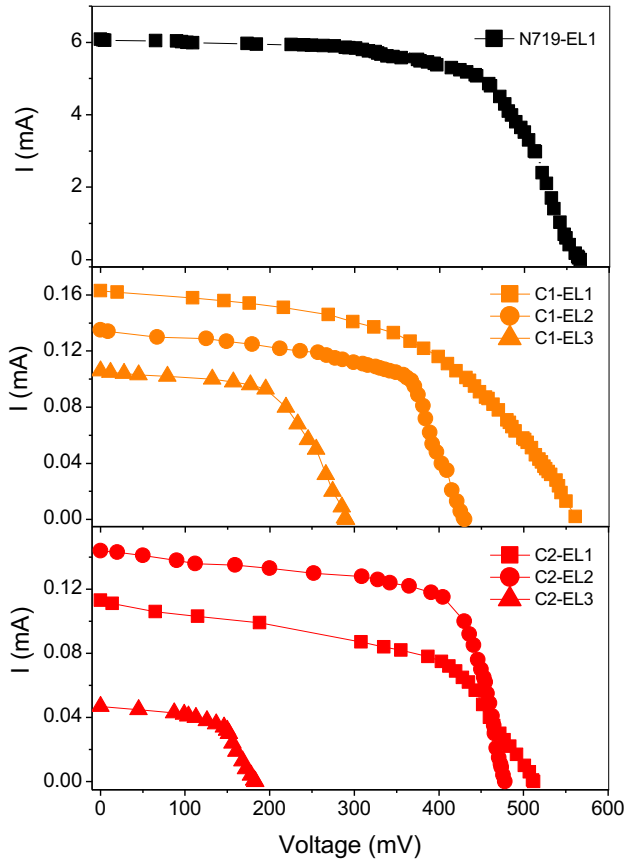

Figure 4. I-V curves for dye-sensitized solar cells made with different dyes: a) N719; (b) Complex 1; c) Complex 2. The cells are characterized using electrolytes 1-3.

The DSCs prepared with the complex $[RuCl_2(mPTA)_3(H_2O)](CF_3SO_3)_3$ and electrolyte 1 (C1-EL1) present a V_{OC}=550 mV, very similar to the value obtained for N719, but a significant lower short circuit current, I_{SC}=0.160 mA. This leads to an overall conversion efficiency η = 0.32 %, which is the best performance achieved with complex 1. These photochemical parameters worsen when complex 1 works in combination with electrolyte 2 (C1-EL2): V_{OC} = 396 mV, I_{SC} = 0.136 mA, η = 0.238 %. The improved performance attained with electrolyte 1 is due to the presence of 4-*tert*-butylpyridine (TBP) affecting the semiconductor-electrolyte interface. It is known that this additive deprotonates the TiO_2 surface by absorption, consequently shifting the conduction band of the semiconductor toward negative potentials [38]. The recombination of the photo-injected electrons and the redox mediator is then reduced. Consequently, the open-circuit potential and thus the overall efficiency of C1-EL1 are improved [39]. With the ionic liquid as electrolyte, the solar cells (C1-EL3) result in even lower photochemical parameters, being V_{OC} = 256 mV, I_{SC} = 0.099 mA, and η = 0.105 %. In this case, the high viscosity of the electrolyte limits the diffusion of the redox mediator and the dye regeneration is therefore not as good as for iodide/triiodide redox couple. This ultimately diminishes the solar cell performance [40], as it is observed in our experiments.

The solar cells sensitized with the complex $[Ru(C{=}C{=}CPh_2)Cp(PTA)(PPh_3)](CF_3SO_3)$ exhibited similar performance than complex 1. The characteristic parameters obtained with electrolyte 1 (C2-EL1) became worse: V_{OC} = 510 mV, I_{SC} = 0.110 mA, η = 0.209 %. Interestingly, the performance improves when using the electrolyte 2 (C2-EL2): V_{OC} = 492 mV, I_{SC} = 0.143 mA, η = 0.330 %. The presence of TBP in this case does not improve the efficiency since it reacts thorough the nitrogen atom with the allenylidene ligand, thus degrading the complex. After the solar exposure, the solar cells changed their characteristic red color (see Figure 1, right) to dark yellow, revealing the nature of this reaction. Despite this disadvantage, the cells C2-EL2 continued working but with a concomitant performance loss. Finally, the cell performance with the ionic liquid electrolyte was poor, yielding an efficiency η= 0.028 %. The reduction in the dye regeneration, in combination with the reactivity of

complex 2 with the nucleophiles of the ionic liquid explain the bad operation of C3-EL3 cells. The reaction of the allenylideneruthenium complex with N-based nucleophiles has been reported elsewhere and support this result [28].

Table 1. Electrical parameters of the DSCs fabricated with the ruthenium complexes (C1, C2) in combination with different electrolytes (EL1-EL3). N719-EL1 stands for the reference cell.

Solar cell	V_{OC} (mV)	I_{SC} (mA)	FF	Efficiency, η (%)
N719-E1	568 ± 1	5.960 ± 0.001	0.63 ± 0.03	10.9 ± 0.6
CI-EL1	550 ± 1	0.160 ± 0.001	0.529 ± 0.011	0.320 ± 0.011
CI-EL2	396 ± 1	0.136 ± 0.001	0.623 ± 0.013	0.238 ± 0.024
CI-EL3	256 ± 1	0.099 ± 0.001	0.575 ± 0.015	0.105 ± 0.024
CII-EL1	510 ± 1	0.110 ± 0.001	0.528 ± 0.006	0.209 ± 0.003
CII-EL2	492 ± 1	0.143 ± 0.001	0.662 ± 0.015	0.330 ± 0.003
CII-EL3	180 ± 1	0.044 ± 0.001	0.50 ± 0.04	0.028 ± 0.004

Comparing the electrical parameters of the different DSCs, fill factors were similar in all cases. Regarding V_{OC} and I_{SC}, the best results were obtained with the iodide/triiodide redox couple. This must be related with the nature of the ruthenium complex and the counter-ions, which make the dye regeneration to be diffusion-limited by the electrolyte viscosity. The highest efficiencies are attained for cells C1-EL1 and C2-EL2, emphasizing the importance of N-based additives, such as TBP, in the cell performance. It is important to note that complex 2 reacts with TPB resulting in smaller photochemical parameters. Overall, the values of the conversion efficiency obtained with the ruthenium complexes are low, despite their good absorption characteristics in the UV-vis. The major drawback seems to be the nature of the ligands that define the HOMO-LUMO energy levels, and then the electron injection controlling the overall performance. More studies are in progress with the aim of further improving the sensitizing properties of these PTA-based ruthenium complexes though a proper design of the ligands.

5. Conclusions

We synthesize two novel ruthenium complexes bearing PTA ligands and use them as photosensitizers in fully operating dye-sensitized solar cells: $[RuCl_2(mPTA)_3(H_2O)](CF_3SO_3)_3$ and $[Ru(C{=}C{=}CPh_2)Cp(PTA)(PPh_3)](CF_3SO_3)$. The presence of PTA ligands makes the complexes soluble in aqueous solvents, which is very interesting for water-based photochemistry. They exhibit excellent absorption properties over a wide range of the spectrum. Complex 1 is characterized by strong absorption peaks at 326 nm and 448 nm, whereas complex 2 displays a peak at 338 nm and a broad and intense absorption band located at 520 nm, similarly to dye N719.

. The performance of DSCs containing the complexes, in combination with three types of electrolyte, is evaluated in comparison with the standard N719. The electrochemical behavior found was similar for both complexes with a strong dependence on the type of the electrolyte. The best performance ($\eta \approx 0.33$ %.) was achieved when using the iodide/triiodide redox mediator. Particularly, complex 2 reacted with the additive 4-tert-butylpyridine (electrolyte 2) reducing the photon-to-light conversion efficiency. The performance of the DSCs was poor compared to the N719 in all cases. Nevertheless, the results demonstrate that ruthenium complexes sensitize the solar cell producing electricity from sunlight while they possess thermal and chemical stability under irradiation.

Acknowledgments: Authors acknowledge the support of Projects CTQ2015-67384-R and CTQ2017-90050-R (MINECO/FEDER). Thanks are also given to Junta de Andalucia PAI-research group FQM-317 and COST Action CM1302 (WG1, WG2). BSM is grateful for the Talent Hub Program co-funded by the European Union's Seventh Framework Program, Marie Skłodowska-Curie actions (Grant Agreement n° 291780), and Junta de Andalucia. AR thanks "Modalidad A of Estancias de profesores e investigadores senior en centros extranjeros, incluido el Programa Salvador de Madariaga" (ref: PRX16/00442; MINECO) for supporting his 6-month stay at STFC Rutherford Appleton Laboratory (UK). AFB thanks the support of the Cernep Research Center; University of Almeria.

Author Contributions: A. Romerosa and A. Fernandez conceived and designed greater part of the experiments. M. Serrano synthesized and characterized the ruthenium complexes. A. Maldonado performed most of the experiments, including AFM and the electrical measurements of the solar cells. B. Sierra analyzed the data and wrote the paper. All the authors contributed equally to the discussion of the data.

Conflicts of Interest: The authors declare no conflict of interest.

References

1. Hagfeldt, A.; Boschloo, G.; Sun, L.; Kloo, L.; Pettersson, H. Dye-sensitized solar cells. *Chem. Rev.* **2010**, *110*, 6595–6663, doi:10.1021/cr900356p.
2. Grätzel, M. Photoelectrochemical cells. *Nature* 2001, *414*, 338–344.
3. Hagfeldt, A.; Boschloo, G.; Sun, L.; Kloo, L.; Pettersson, H. Dye-Sensitized Solar Cells. *Chem. Rev.* **2010**, *110*, 6595–6663, doi:10.1021/cr9003049.
4. Polizzotti, A.; Schual-berke, J.; Falsgraf, E.; Johal, M. 5. Investigating New Materials and Architectures for Grätzel Cells. *Third Gener. Photovoltaics* **2012**, doi:10.5772/28223.
5. Hara, K.; Arakawa, H. Dye-sensitized solar cells. In *Handbook of Photovoltaic Science and Engineering*; 2003; p. pages 663–700 ISBN 9780470014004.
6. Calogero, G.; Yum, J. H.; Sinopoli, A.; Di Marco, G.; Grätzel, M.; Nazeeruddin, M. K. Anthocyanins and betalains as light-harvesting pigments for dye-sensitized solar cells. *Sol. Energy* **2012**, *86*, 1563–1575, doi:10.1016/j.solener.2012.02.018.
7. O'Regan, B.; Grätzel, M. A low-cost, high-efficiency solar cell based on dye-sensitized colloidal TiO2 films. *Nature* **1991**, *353*, 737–740, doi:10.1038/353737a0.
8. Sekar, N.; Gehlot, V. Y. Metal complex dyes for dye-sensitized solar cells: Recent developments. *Resonance* **2010**, *15*, 819–831, doi:10.1007/s12045-010-0091-8.
9. Nazeeruddin, M. K.; Kay, A.; Rodicio, I.; Humphry-Baker, R.; Mueller, E.; Liska, P.; Vlachopoulos, N.; Graetzel, M. Conversion of light to electricity by cis-X2bis(2,2′-bipyridyl-4,4′-dicarboxylate)ruthenium(II) charge-transfer sensitizers (X = Cl-, Br-, I-, CN-, and SCN-) on nanocrystalline titanium dioxide electrodes. *J. Am. Chem. Soc.* **1993**, *115*, 6382–6390, doi:10.1021/ja00067a063.
10. Wang, Z. S.; Yamaguchi, T.; Sugihara, H.; Arakawa, H. Significant efficiency improvement of the black dye-sensitized solar cell through protonation of TiO2films. *Langmuir* **2005**, *21*, 4272–4276, doi:10.1021/la050134w.
11. Chiba, Y.; Islam, A.; Watanabe, Y.; Komiya, R.; Koide, N.; Han, L. Dye-Sensitized Solar Cells with Conversion Efficiency of 11.1%. *Jpn. J. Appl. Phys.* **2006**, *45*, L638–L640, doi:10.1143/JJAP.45.L638.
12. Robertson, N. Optimizing dyes for dye-sensitized solar cells. *Angew. Chem. Int. Ed.* **2006**, *45*, 2338–2345, doi:10.1002/anie.200503083.
13. Polo, A. S.; Itokazu, M. K.; Murakami Iha, N. Y. Metal complex sensitizers in dye-sensitized solar cells. *Coord. Chem. Rev.* 2004, *248*, 1343–1361.
14. Spiccia, L.; Deacon, G. B.; Kepert, C. M. Synthetic routes to homoleptic and heteroleptic ruthenium(II) complexes incorporating bidentate imine ligands. *Coord. Chem. Rev.* 2004, *248*, 1329–1341.
15. Vougioukalakis, G. C.; Philippopoulos, A. I.; Stergiopoulos, T.; Falaras, P. Contributions to the development of ruthenium-based sensitizers for dye-sensitized solar cells. *Coord. Chem. Rev.* 2011, *255*, 2602–2621.
16. Reynal, A.; Palomares, E. Ruthenium polypyridyl sensitisers in dye solar cells based on mesoporous TiO2. *Eur. J. Inorg. Chem.* 2011, 4509–4526.

17. Qin, Y.; Peng, Q. Ruthenium sensitizers and their applications in dye-sensitized solar cells. *Int. J. Photoenergy* 2012, *2012*.
18. Bomben, P. G.; Robson, K. C. D.; Koivisto, B. D.; Berlinguette, C. P. Cyclometalated ruthenium chromophores for the dye-sensitized solar cell. *Coord. Chem. Rev.* 2012, *256*, 1438–1450.
19. Johansson, E. M. J.; Sandell, A.; Siegbahn, H.; Rensmo, H.; Mahrov, B.; Boschloo, G.; Figgemeier, E.; Hagfeldt, A.; Jönsson, S. K. M.; Fahlman, M. Interfacial properties of photovoltaic TiO2/dye/PEDOT-PSS heterojunctions. *Synth. Met.* **2005**, *149*, 157–167, doi:10.1016/j.synthmet.2004.12.004.
20. Joó, F.; Kovács, J.; Kathó, Á.; Bényei, A. C.; Decuir, T.; Darensbourg, D. J.; Miedaner, A.; Dubois, D. L. (Meta- Sulfonatophenyl) Diphenylphosphine, Sodium Salt and its Complexes with Rhodium(I), Ruthenium(II), Iridium(I). In *Inorganic Syntheses*; 2007; pp. 1–8 ISBN 9780470132630.
21. Hallman, P. S.; Stephenson, T. A.; Wilkinson, G. Tetrakis(triphenylphosphine)dichlororuthenium(II) and Tris(triphenylphosphine)dichlororuthenium(II). In *Inorganic Syntheses, Volume XII*; 1970; pp. 237–40 ISBN 9780470132432.
22. *Aqueous-Phase Organometallic Catalysis*; B. Cornils and W.A. Hermans, Ed.; Wiley-VCH: Weinheim, Germany, 1998;
23. Akbayeva, D. N.; Gonsalvi, L.; Oberhauser, W.; Peruzzini, M.; Vizza, F.; Brüggeller, P.; Romerosa, A.; Sava, G.; Bergamo, A. Synthesis, catalytic properties and biological activity of new water soluble ruthenium cyclopentadienyl PTA complexes [(C5R5)RuCl(PTA)2] (R = H, Me; PTA = 1,3,5-triaza-7-phosphaadamantane). *Chem. Commun. (Camb).* **2003**, 264–265, doi:10.1039/B210102E.
24. Romerosa, A.; Campos-Malpartida, T.; Lidrissi, C.; Saoud, M.; Serrano-Ruiz, M.; Peruzzini, M.; Garrido-Cárdenas, J. A.; García-Maroto, F. Synthesis, characterization, and DNA binding of new water-soluble cyclopentadienyl ruthenium(II) complexes incorporating phosphines. *Inorg. Chem.* **2006**, *45*, 1289–1298, doi:10.1021/ic051053q.
25. Romerosa, A.; Saoud, M.; Campos-Malpartida, T.; Lidrissi, C.; Serrano-Ruiz, M.; Peruzzini, M.; Garrido, J. A.; García-Maroto, F. DNA interactions mediated by cyclopentadienidoruthenium(II) complexes containing water-soluble phosphanes. *Eur. J. Inorg. Chem.* **2007**, 2803–2812, doi:10.1002/ejic.200601177.
26. Girotti, R.; Romerosa, A.; Mañas, S.; Serrano-Ruiz, M.; Perutz, R. Photo-aquation of cis-[RuCl2(mPTA)4](CF3SO3)4 in water (mPTA = N-methyl-1,3,5-triaza-7-phosphaadamantane). *Dalton Trans.* **2011**, *40*, 828–36, doi:10.1039/c0dt00885k.
27. Smoleński, P.; Pruchnik, F. P.; Ciunik, Z.; Lis, T. New rhodium(III) and ruthenium(II) water-soluble complexes with 3,5-diaza-1-methyl-1-azonia-7-phosphatricyclo[3.3.1.13,7decane. *Inorg. Chem.* **2003**, *42*, 3318–3322, doi:10.1021/ic034044v.
28. Serrano-Ruiz, M.; Lidrissi, C.; Mañas, S.; Peruzzini, M.; Romerosa, A. Synthesis, reactivity and catalytic properties of the allenylidene [Ru(C=C=CPh2)Cp(PTA)(PPh3)](CF3SO3) (PTA = 1,3,5-triaza-7-phosphaadamantane). *J. Organomet. Chem.* **2014**, *751*, 654–661, doi:10.1016/j.jorganchem.2013.08.040.
29. Ramadan, A. A.; Gould, R. D.; Ashour, A. On the Van der Pauw method of resistivity measurements. *Thin Solid Films* **1994**, *239*, 272–275, doi:10.1016/0040-6090(94)90863-X.
30. Longo, C.; De Paoli, M. A. Dye-Sensitized Solar Cells: A Successful Combination of Materials. In *Journal of the Brazilian Chemical Society*; 2003; Vol. 14, pp. 889–901.
31. Maldonado-Valdivia, A. I.; Galindo, E. G.; Ariza, M. J.; García-Salinas, M. J. Surfactant influence in the performance of titanium dioxide photoelectrodes for dye-sensitized solar cells. *Sol. Energy* **2013**, *91*, 263–272, doi:10.1016/j.solener.2013.02.009.
32. Ito, S. Facile fabrication of mesoporous TiO2 electrodes for dye solar cells: chemical modification and

repetitive coating. *Sol. Energy Mater. Sol. Cells* **2003**, *76*, 3–13, doi:10.1016/S0927-0248(02)00209-X.

33. Ito, S.; Murakami, T. N.; Comte, P.; Liska, P.; Grätzel, C.; Nazeeruddin, M. K.; Grätzel, M. Fabrication of thin film dye sensitized solar cells with solar to electric power conversion efficiency over 10%. *Thin Solid Films* **2008**, *516*, 4613–4619, doi:10.1016/j.tsf.2007.05.090.
34. Hirata, N.; Lagref, J. J.; Palomares, E. J.; Durrant, J. R.; Nazeeruddin, M. K.; Gratzel, M.; Di Censo, D. Supramolecular Control of Charge-Transfer Dynamics on Dye-sensitized Nanocrystalline TiO2Films. *Chem. - A Eur. J.* **2004**, *10*, 595–602, doi:10.1002/chem.200305408.
35. Tsai, C. H.; Hsu, S. Y.; Lu, C. Y.; Tsai, Y. T.; Huang, T. W.; Chen, Y. F.; Jhang, Y. H.; Wu, C. C. Influences of textures in Pt counter electrode on characteristics of dye-sensitized solar cells. *Org. Electron. physics, Mater. Appl.* **2012**, *13*, 199–205, doi:10.1016/j.orgel.2011.10.020.
36. Nogueira, A. F.; Longo, C.; De Paoli, M. A. Polymers in dye sensitized solar cells: Overview and perspectives. *Coord. Chem. Rev.* 2004, *248*, 1455–1468.
37. Wang, Z.-S.; Kawauchi, H.; Kashima, T.; Arakawa, H. Significant influence of TiO2 photoelectrode morphology on the energy conversion efficiency of N719 dye-sensitized solar cell. *Coord. Chem. Rev.* **2004**, *248*, 1381–1389, doi:10.1016/j.ccr.2004.03.006.
38. Boschloo, G.; Häggman, L.; Hagfeldt, A. Quantification of the effect of 4-tert-butylpyridine addition to I -/I3- redox electrolytes in dye-sensitized nanostructured TiO2 solar cells. *J. Phys. Chem. B* **2006**, *110*, 13144–13150, doi:10.1021/jp0619641.
39. Nakade, S.; Kanzaki, T.; Kubo, W.; Kitamura, T.; Wada, Y.; Yanagida, S. Role of electrolytes on charge recombination in dye-sensitized TiO(2) solar cell (1): the case of solar cells using the I(-)/I(3)(-) redox couple. *J. Phys. Chem. B* **2005**, *109*, 3480–7, doi:10.1021/jp0460036.
40. Cheng, P.; Wang, W.; Lan, T.; Chen, R.; Wang, J.; Yu, J.; Wu, H.; Yang, H.; Deng, C.; Guo, S. Electrochemical characterization and photovoltaic performance of the binary ionic liquid electrolyte of 1-methyl-3-propylimidazolium iodide and 1-ethyl-3-methylimidazolium tetrafluoroborate for dye-sensitized solar cells. *J. Photochem. Photobiol. A Chem.* **2010**, *212*, 147–152, doi:10.1016/j.jphotochem.2010.04.009.